Revealing the effect of altered diffusion paths by excess Al^{3+} preinsertion on the performance of zinc-ion batteries

Lingli Xing[a,b], Chengyi Zhang[c], Ming Li[a], Ping Hu[a], Xinyu Zhang[a], Yuhang Dai[a], Xuelei Pan[a], Weiyi Sun[a], Shanlin Li[b], Junmin Xue[b], Qinyou An[a,d,] and Liqiang Mai[a,d,*]*

[a] State Key Laboratory of Advanced Technology for Materials Synthesis and Processing, Wuhan University of Technology, Wuhan 430070, P. R. China

[b] Department of Materials Science and Engineering, National University of Singapore, 117575, Singapore

[c] Institute of Technological Sciences, Wuhan University, Wuhan 430072, P. R. China

[d] Foshan Xianhu Laboratory of the Advanced Energy Science and Technology Guangdong Laboratory, Xianhu hydrogen Valley, Foshan 528200, P. R. China

E-mail: anqinyou86@whut.edu.cn (Prof. Qinyou An); mlq518@whut.edu.cn (Prof. Liqiang Mai)

4.3. Material characterization

X-ray diffraction (XRD) measurement was measured using a Bruker D8 Discover X-ray diffractometer with the non-monochromatic Cu Kα X-ray as the source (λ = 1.5406 Å). Inductively coupled plasma (ICP) measurement was recorded with a PerkinElmer Optima 4300DV spectrometer. Raman spectra were obtained using a HORIBA LabRAM HR Evolution micro-Raman spectroscopy system with an excitation laser wavelength of λ = 532 nm. Thermogravimetric analysis (TGA) curves were conducted by using a Netzsch STA 449C simultaneous analyzer. Fourier transform infrared (FTIR) spectra were performed using a Nicolet 6700 (Thermo Fisher Scientific Co., USA) IR spectrometer. The Brunauer-Emmett-Teller (BET) surface area was collected through Tristar II 3020 instrument at 77 K. Scanning electron microscopy (SEM) images were carried out on a JEOL-7100F scanning electron microscope. Transmission electron microscopy (TEM) and high-resolution TEM (HRTEM) images were obtained with a JEM-2100F STEM/EDS microscope. X-ray photoelectron spectroscopy (XPS) spectra were conducted with a VG Multi Lab 2000 instrument.

4.4. Computation methods

All DFT calculations were carried out by the CASTEP module in the Materials Studio. The cut-off energy for the plane-wave expansion was set as 550 eV, the *Γ*-centered *k*-mesh was adopted as 3×3×3 for the geometry optimization of all structures. The criteria of convergence for max force, stress, and displacement were 0.02 eV/A, 0.03 GPa, and 0.001 Å, individually. The Perdew-Burke-Ernzerh of generalized gradient approximation (GGA) was performed,[1] and the ultrasoft pseudopotential for every atom was adopted.[2]

The original V_2O_5 structure is constructed from the crystalline structure database and experimental results. To explain the migration behavior of the Zn^{2+} ions in the anode, we calculate the migration barrier when the Zn^{2+} ions transfer at the bulk structure of AVO with different ratios of doped Al^{3+}. The complete linear synchronous transit (LST) and quadratic synchronous transit (QST) methods[3-5] were employed to search the transition state (TS), where the cut-off energy, SCF convergence, max force, stress, displacement are set as 550 eV, 2.0×10^{-5} eV/atom, 0.02 eV/Å, 0.1 GPa, and 0.002 Å, individually.

Sample	Mass ratio (Al:V)	Al atomic number/per cell
1	0.1670	10.1
2	0.1818	11.0
3	0.1867	11.3
4	0.2078	12.5

Table S1. ICP measurement results and Al atomic number of HAVOs.

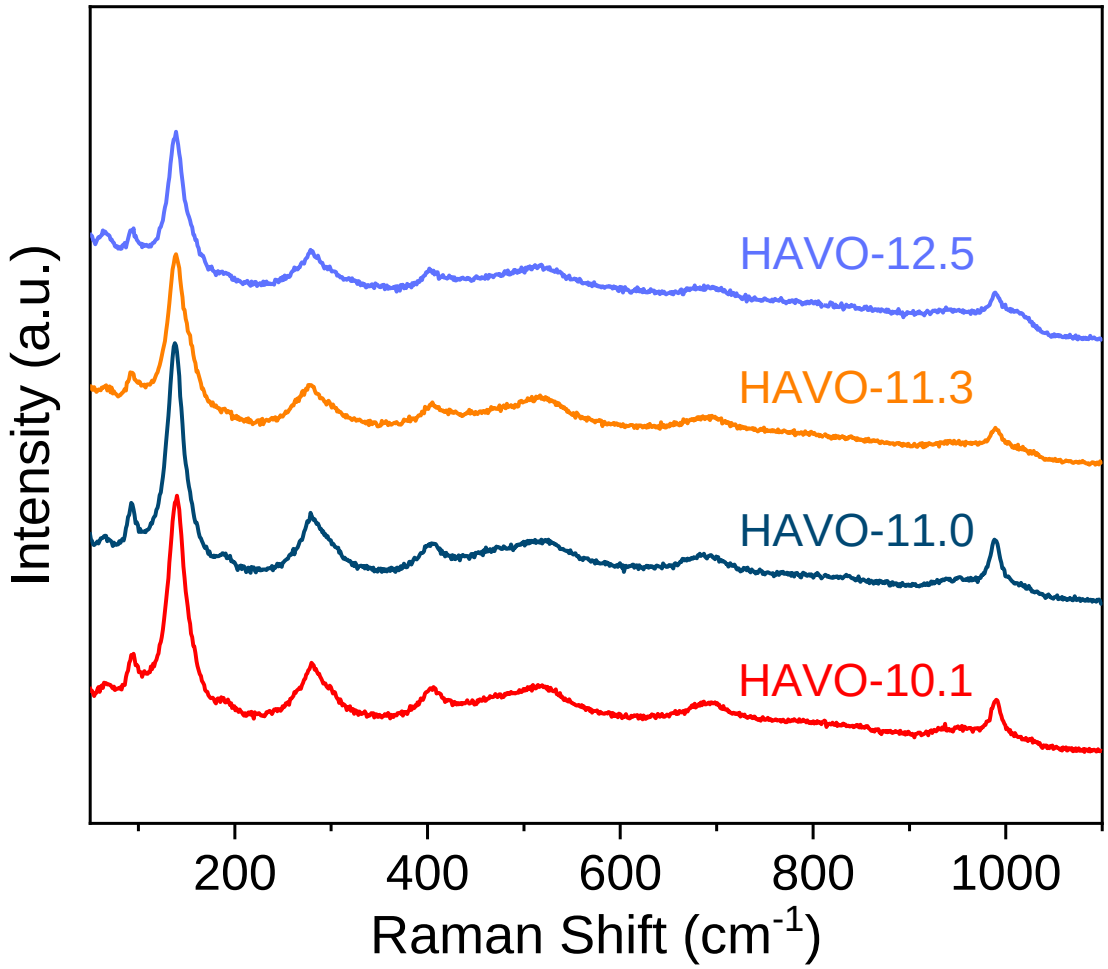

Figure S1. Raman spectra of HAVOs.

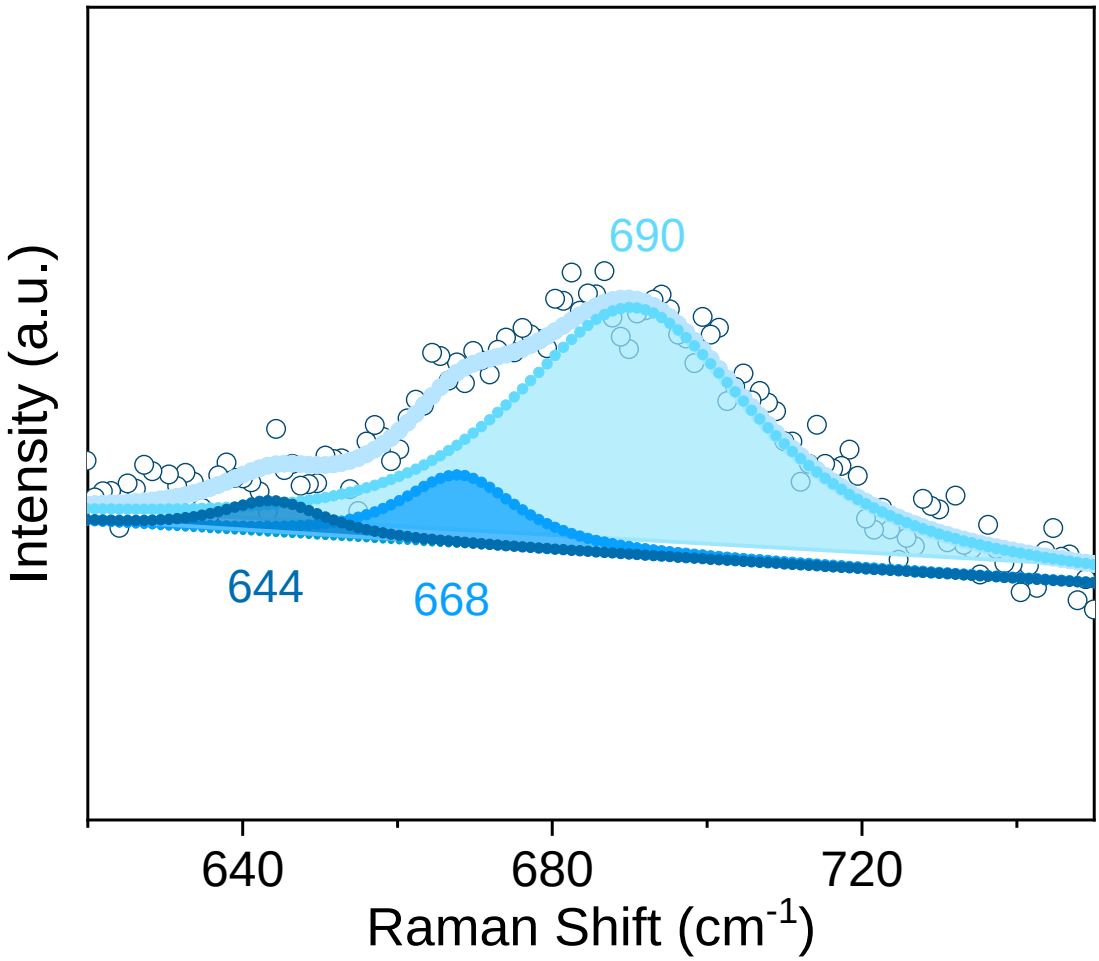

Figure S2. The partially fitted Raman spectrum from 620 to 760 cm^{-1} of HAVO-11.0.

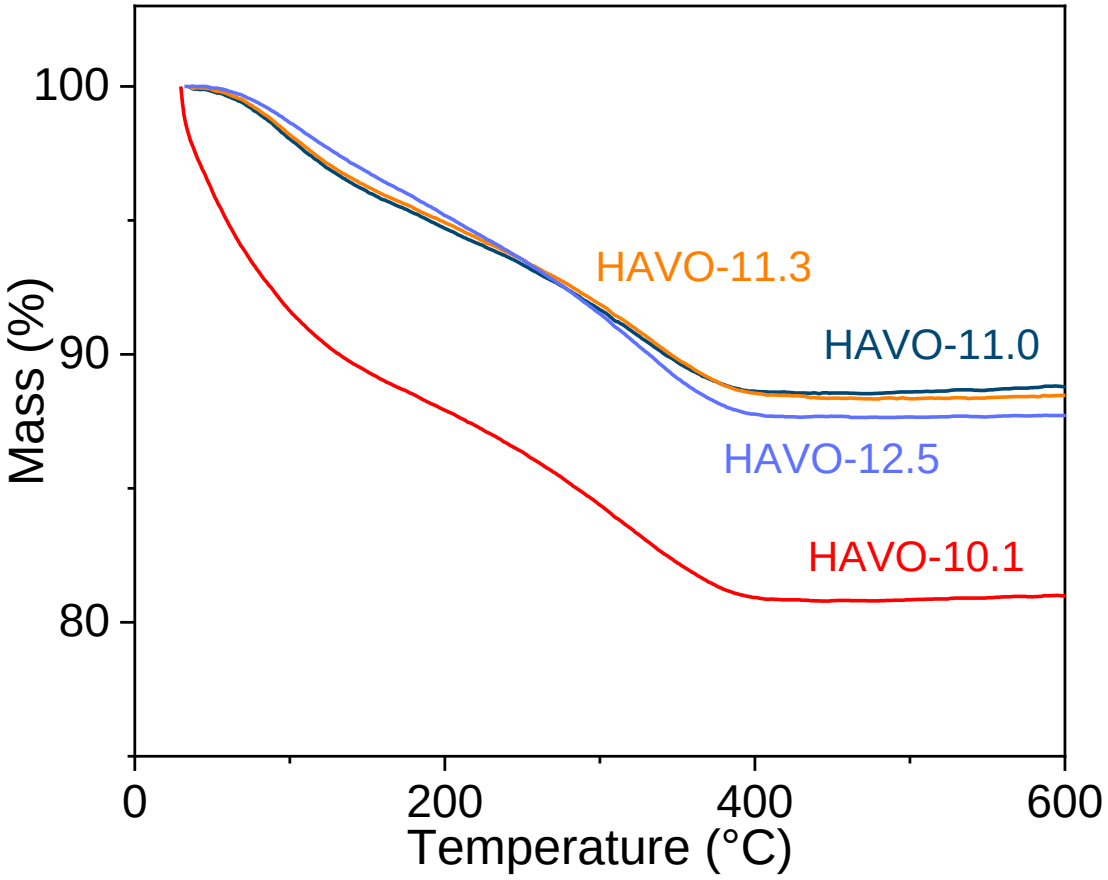

Figure S3. TGA curves of HAVOs.

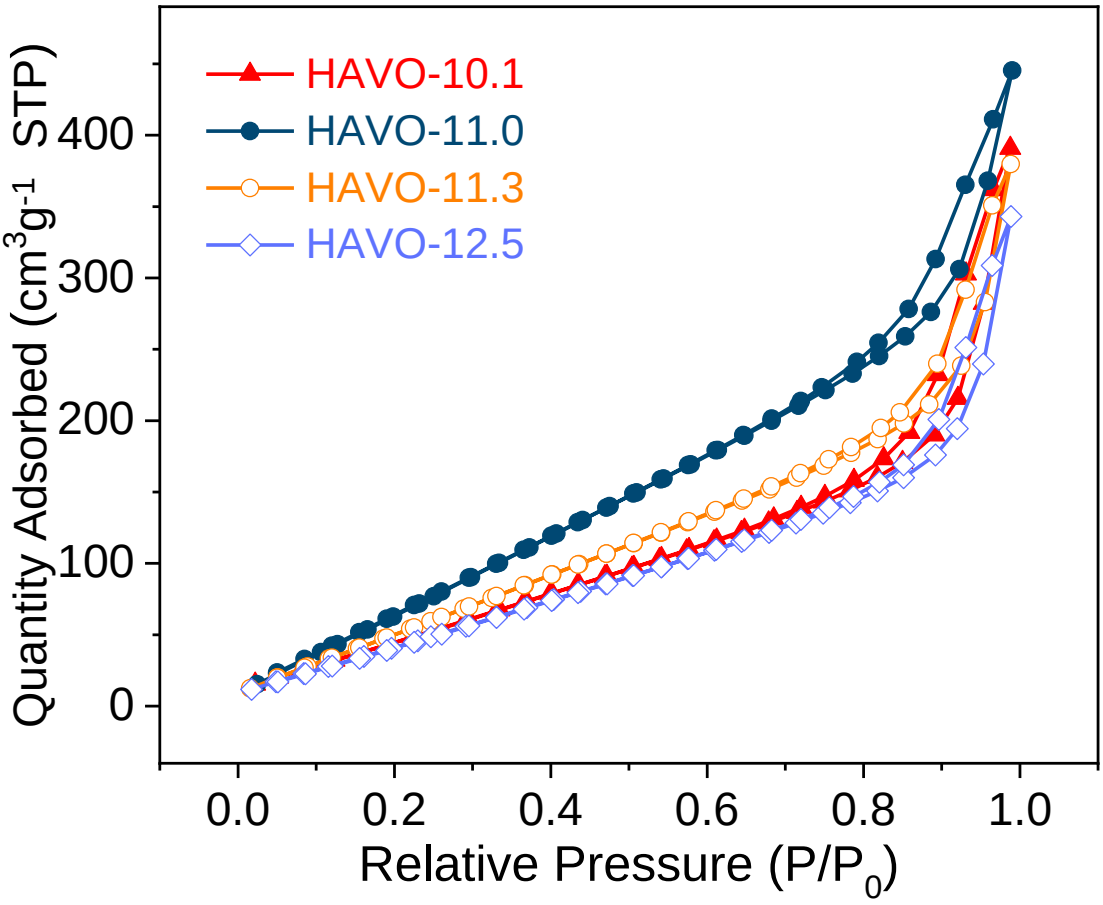

Figure S4. N_2 adsorption-desorption isotherm curves of HAVOs.

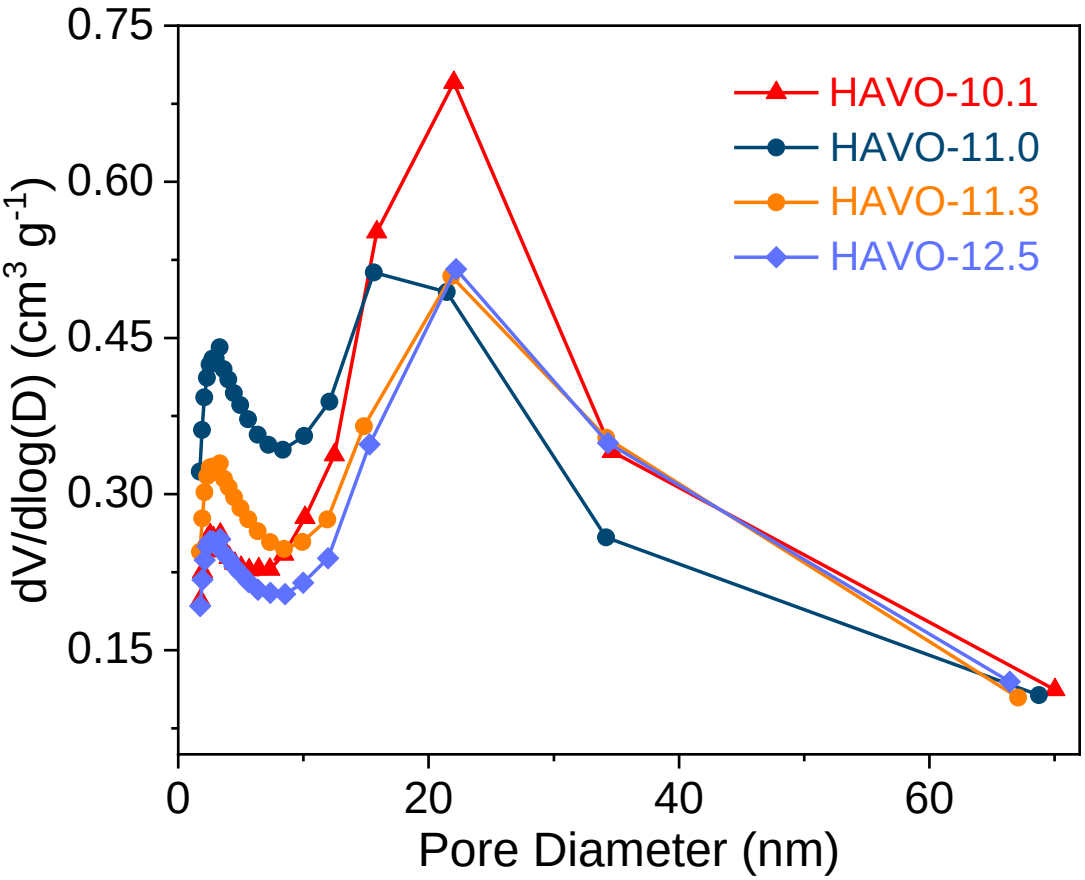

Figure S5. Pore diameter distribution curves of HAVOs.

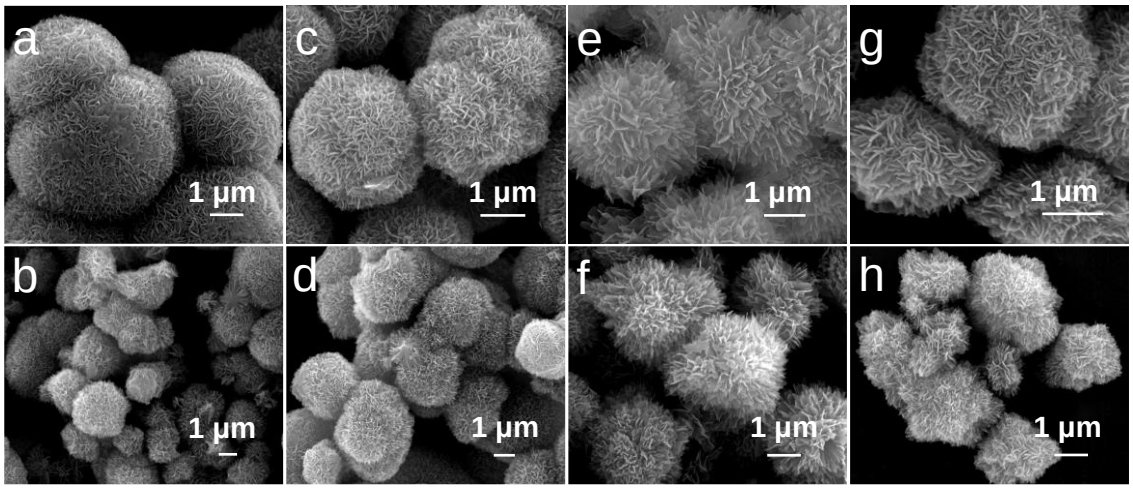

Figure S6. Typical SEM images of HAVO-10.1 (a, b), HAVO-11.0 (c, d), HAVO-11.3 (e, f) and HAVO-12.5 (g, h).

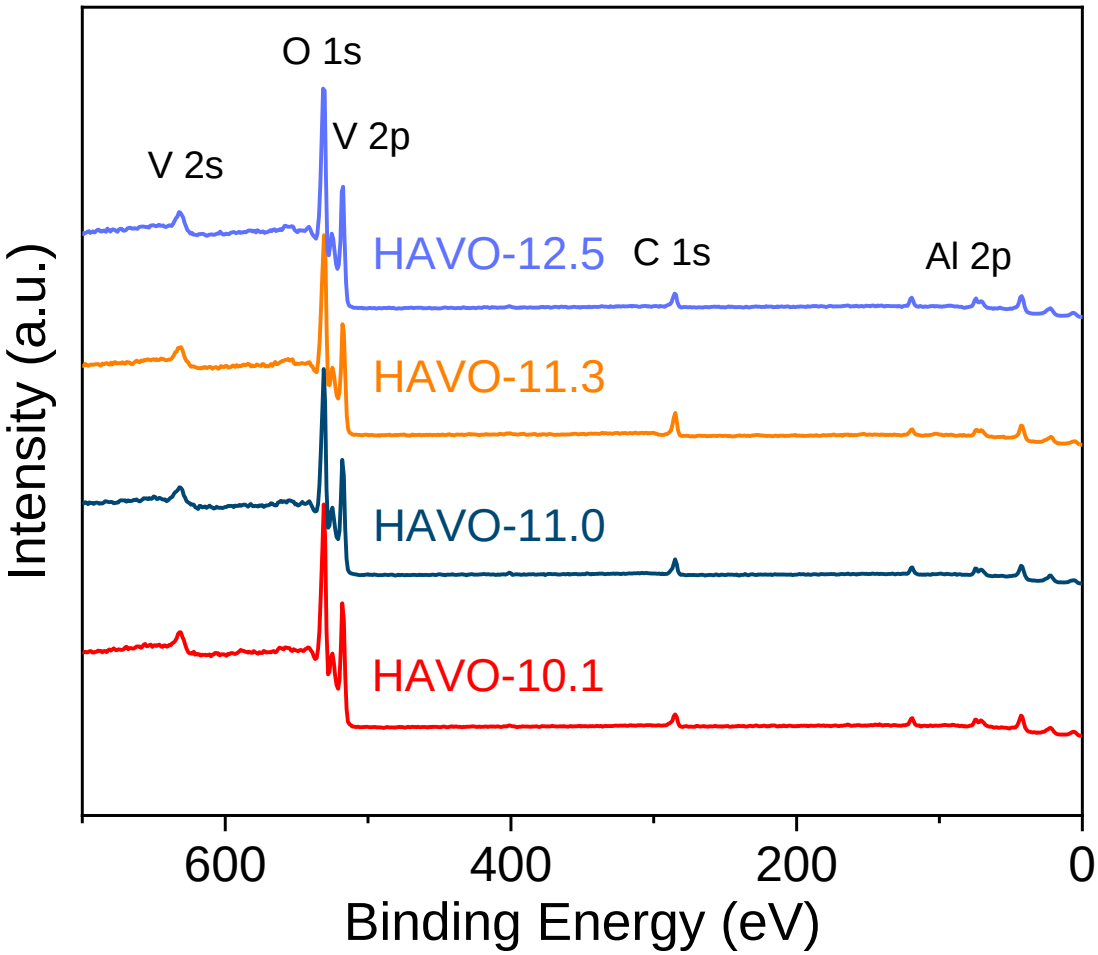

Figure S7. Full survey XPS spectra of HAVOs.

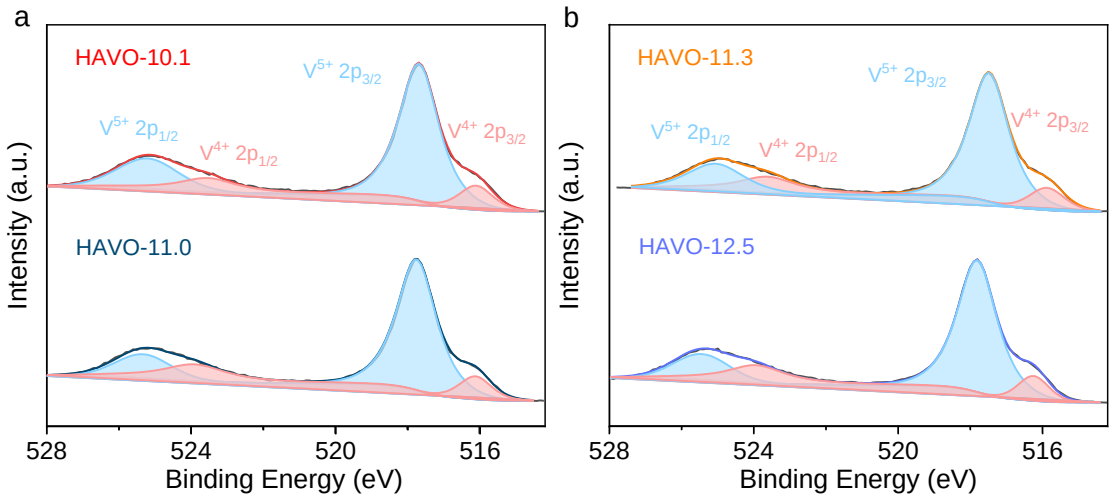

Figure S8. High-resolution V 2p XPS spectra of HAVOs.

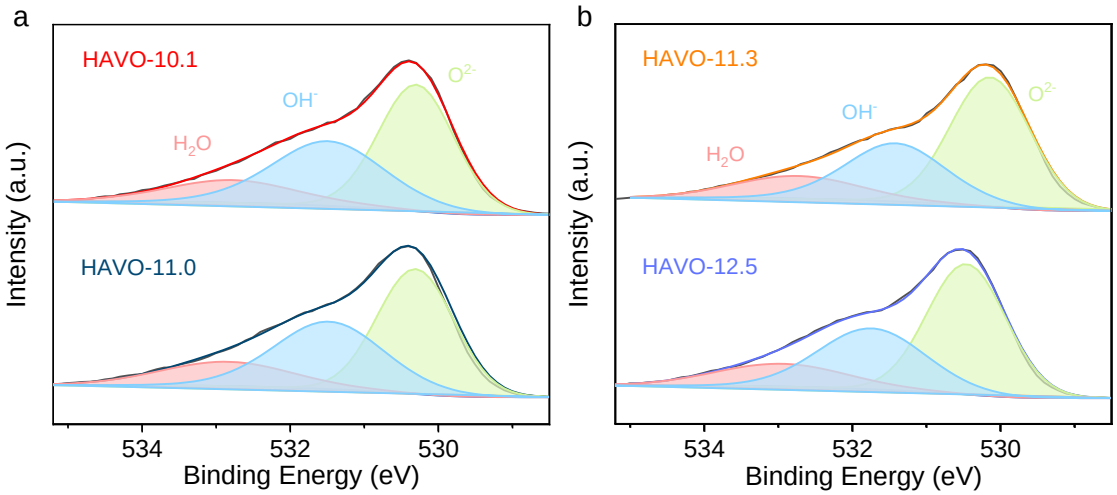

Figure S9. High-resolution O 1s XPS spectra of HAVOs.

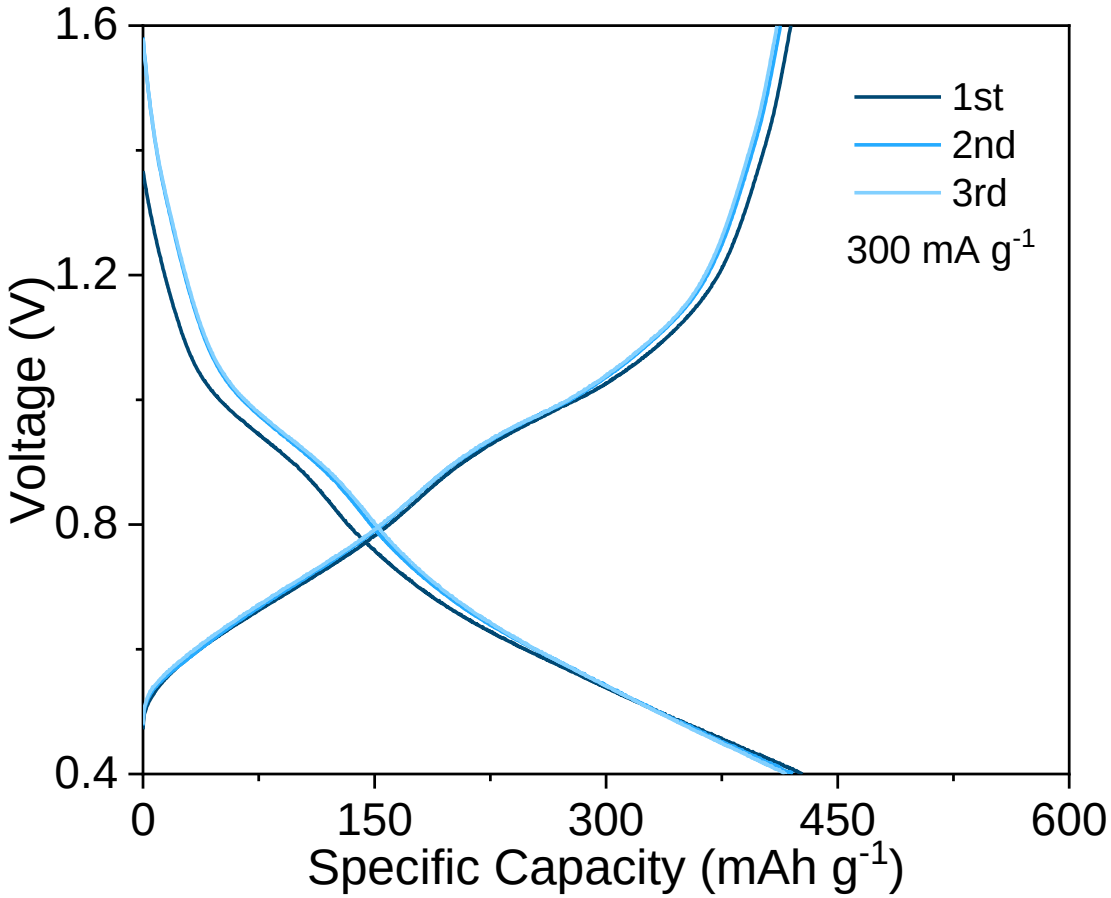

Figure S10. Representative charge/discharge curves of HAVO-11.0 at 300 mA g^{-1}.

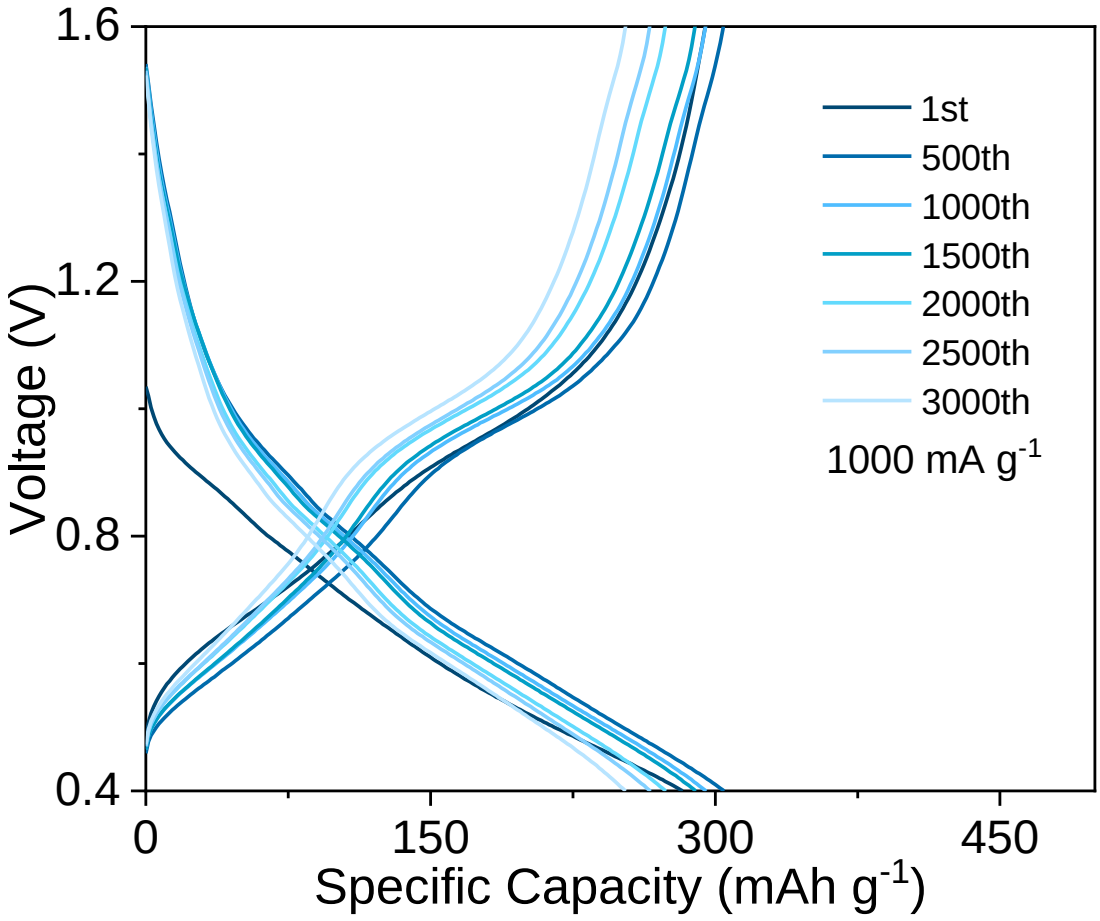

Figure S11. Representative charge/discharge curves of HAVO-11.0 at 1000 mA g^{-1}.

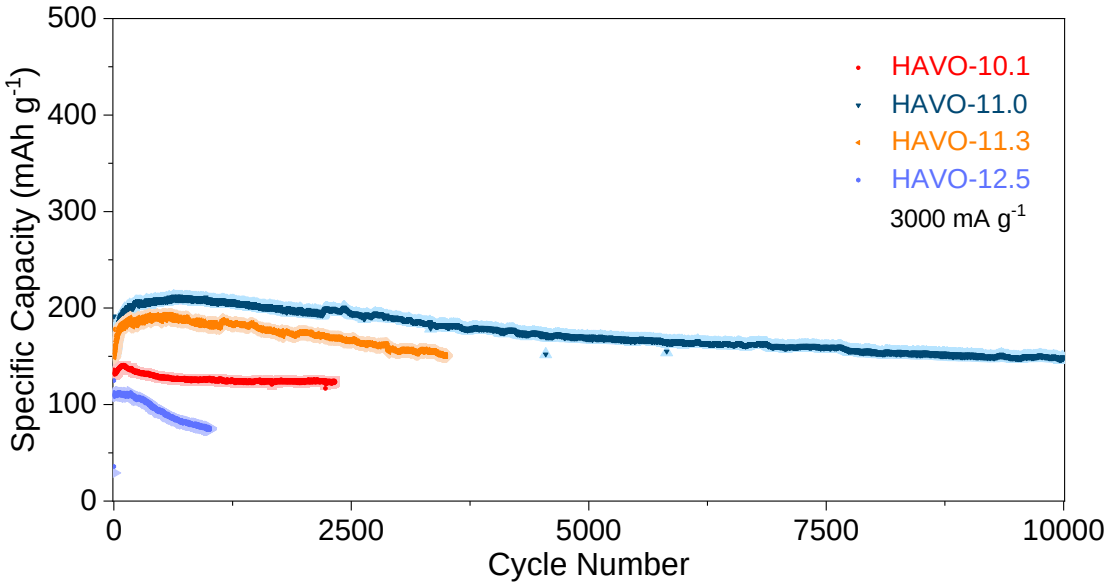

Figure S12. Cycling performances tested of HAVOs at 3000 mA g^{-1}.

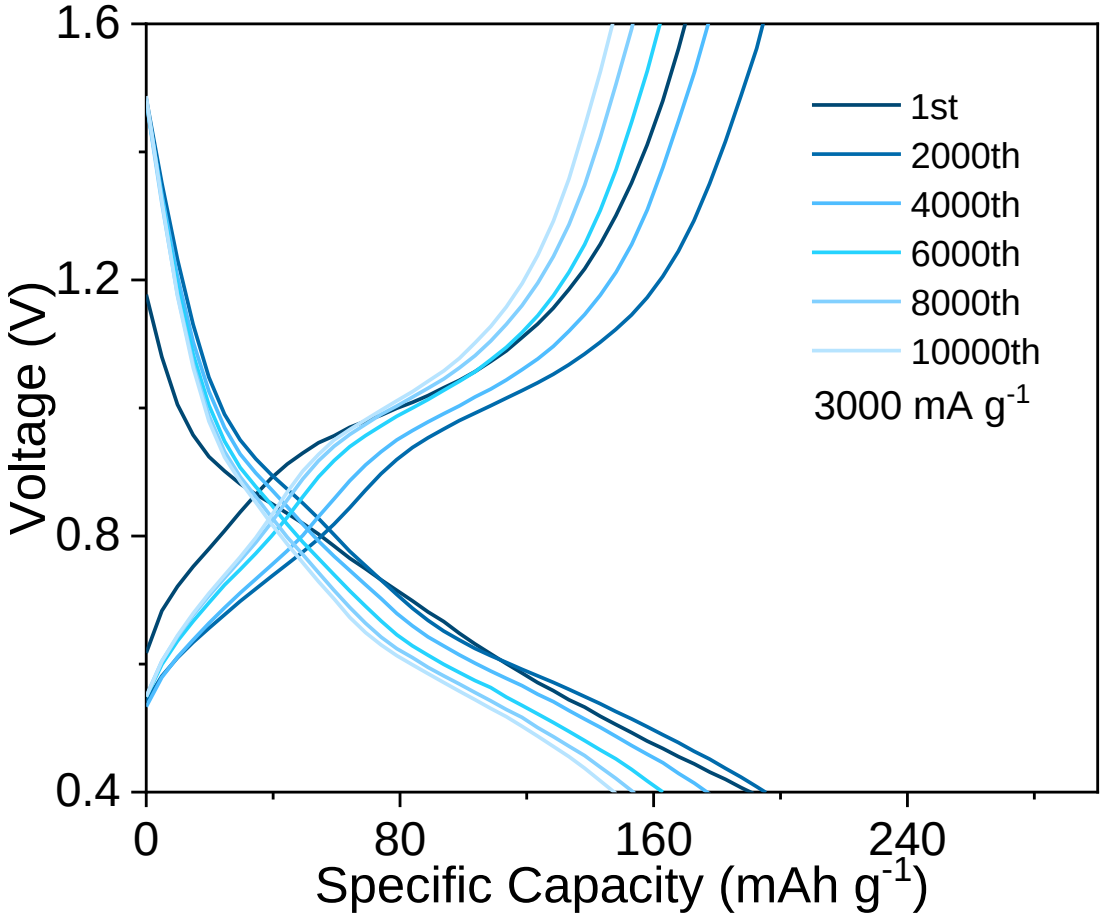

Figure S13. Representative charge/discharge curves of HAVO-11.0 at 3000 mA g^{-1}.

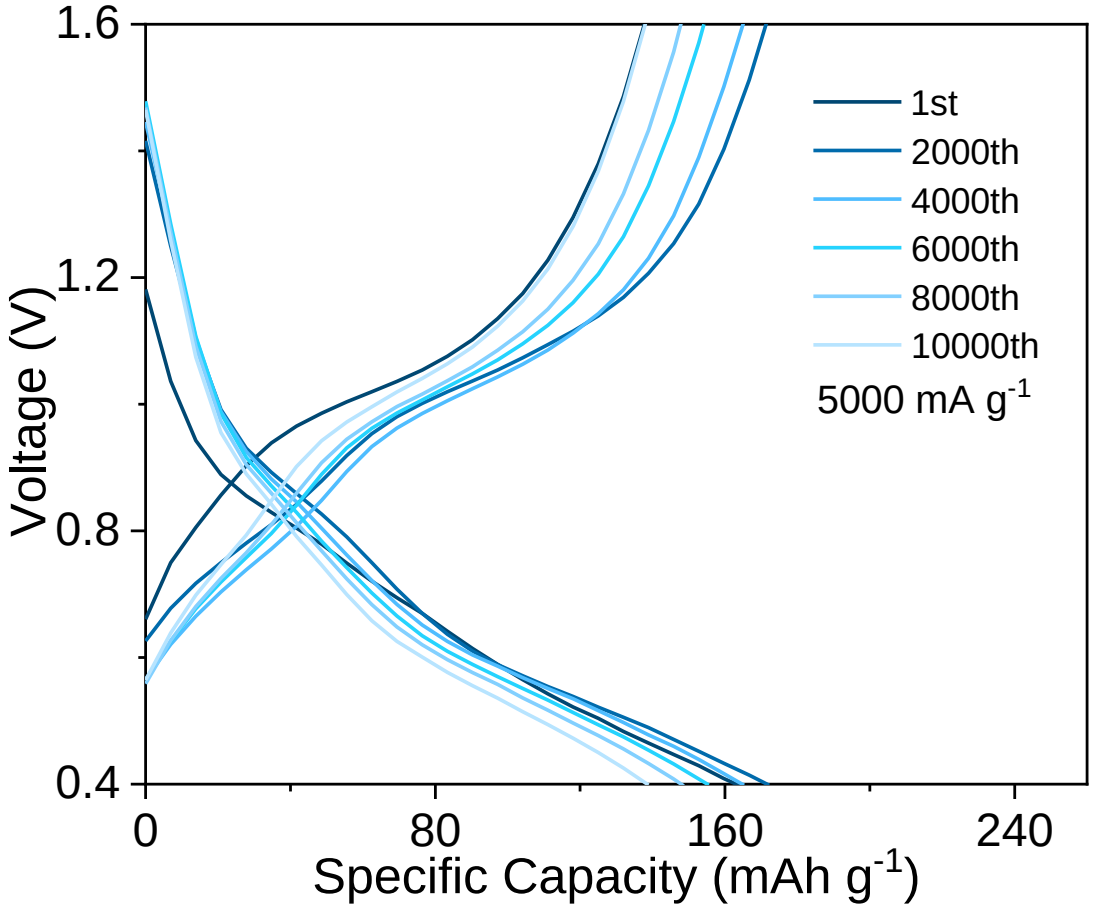

Figure S14. Representative charge/discharge curves of HAVO-11.0 at 5000 mA g^{-1}.

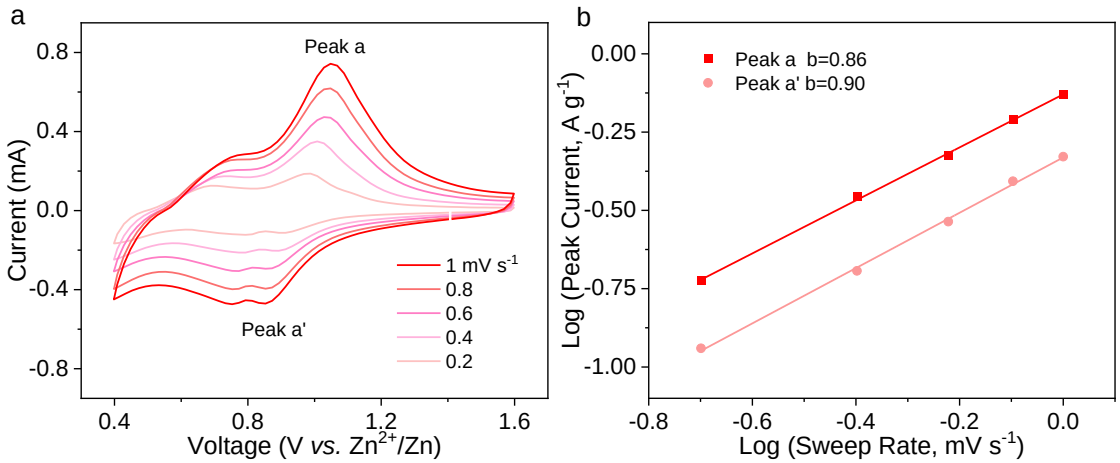

Figure S15. (a) CV curves of HAVO-10.1 at different scan rates. (b) The plots of log (peak current) versus log (sweep rate) at each peak from CV curves of HAVO-10.1.

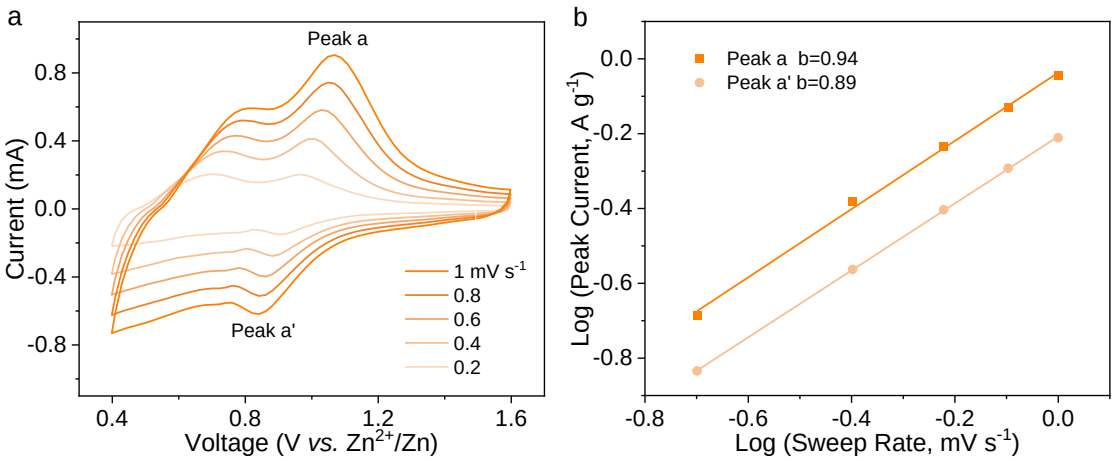

Figure S16. (a) CV curves of HAVO-11.3 at different scan rates. (b) The plots of log (peak current) versus log (sweep rate) at each peak from CV curves of HAVO-11.3.

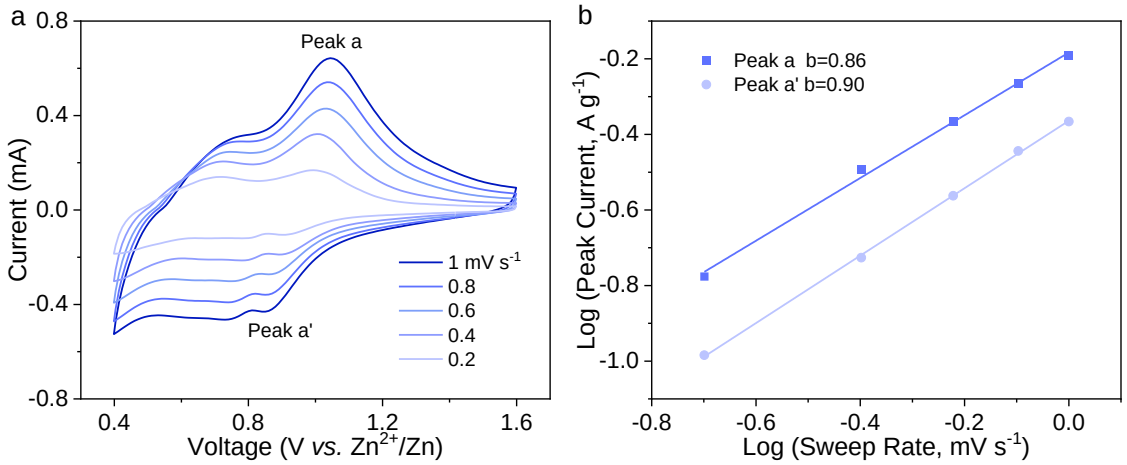

Figure S17. (a) CV curves of HAVO-12.5 at different scan rates. (b) The plots of log (peak current) versus log (sweep rate) at each peak from CV curves of HAVO-12.5.

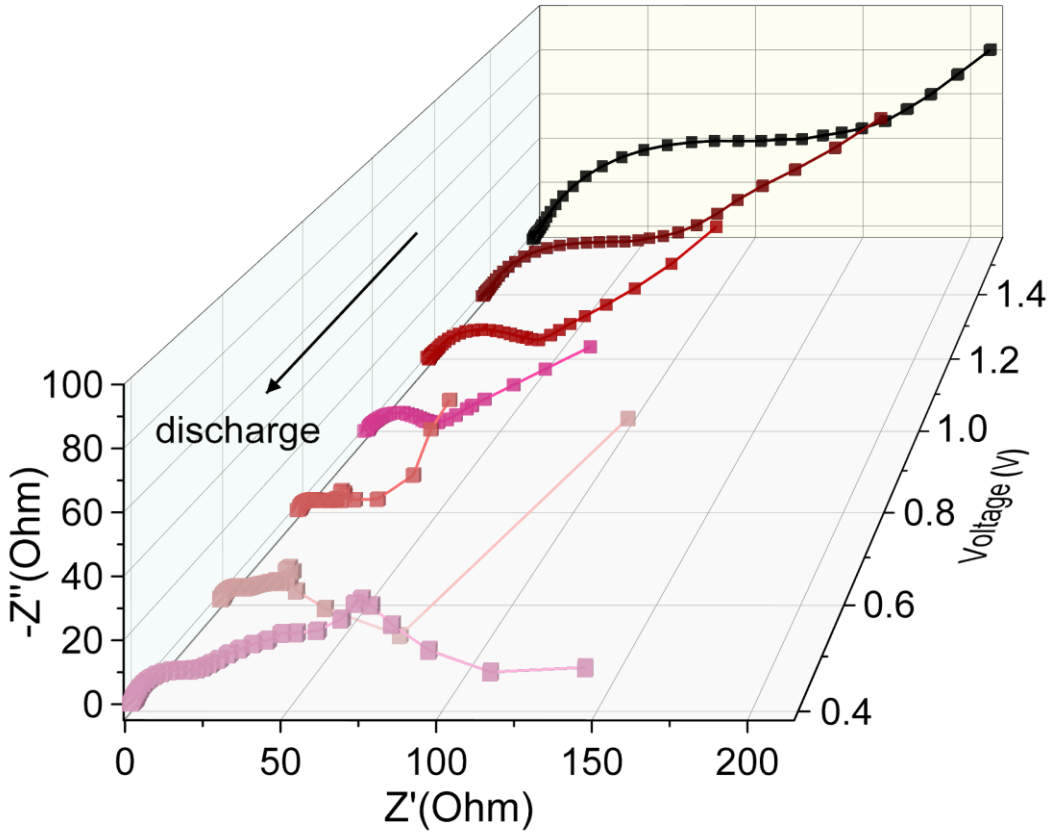

Figure S18. *In-situ* impedance spectra of HAVO-11.0 cathode at 100 mA g^{-1} during the first discharge process.

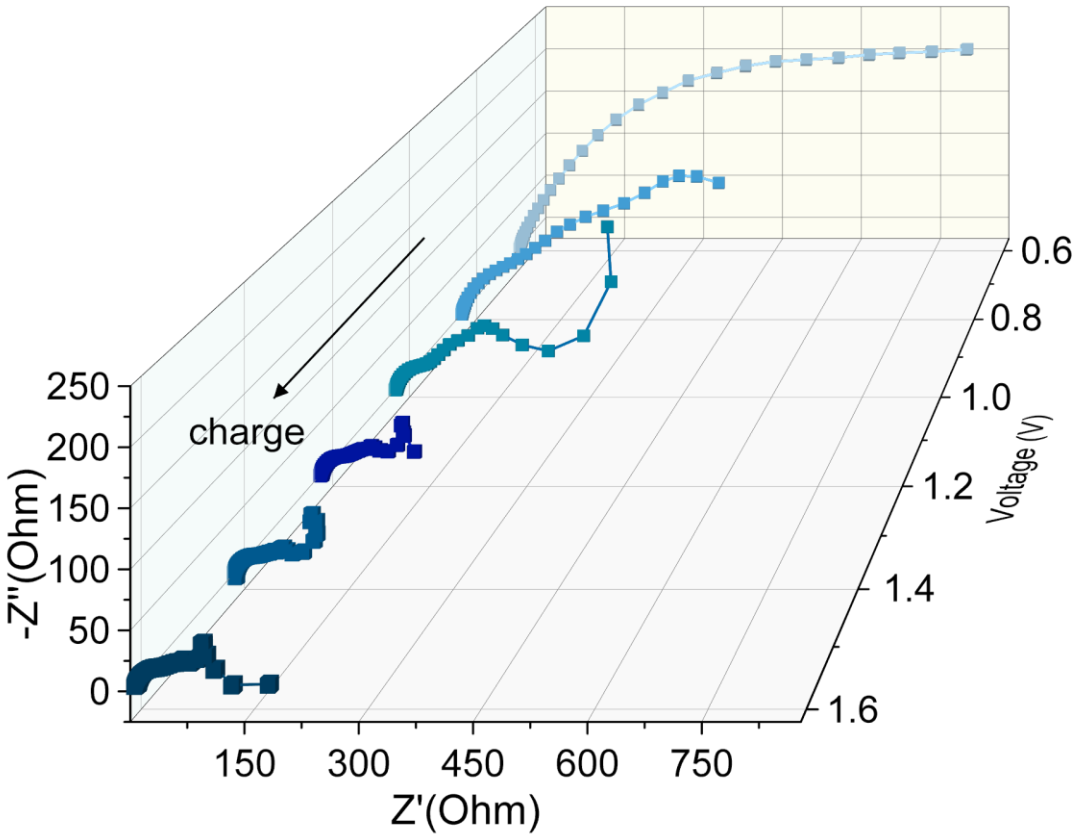

Figure S19. *In-situ* impedance spectra of HAVO-11.0 cathode at 100 mA g^{-1} during the first charge process.

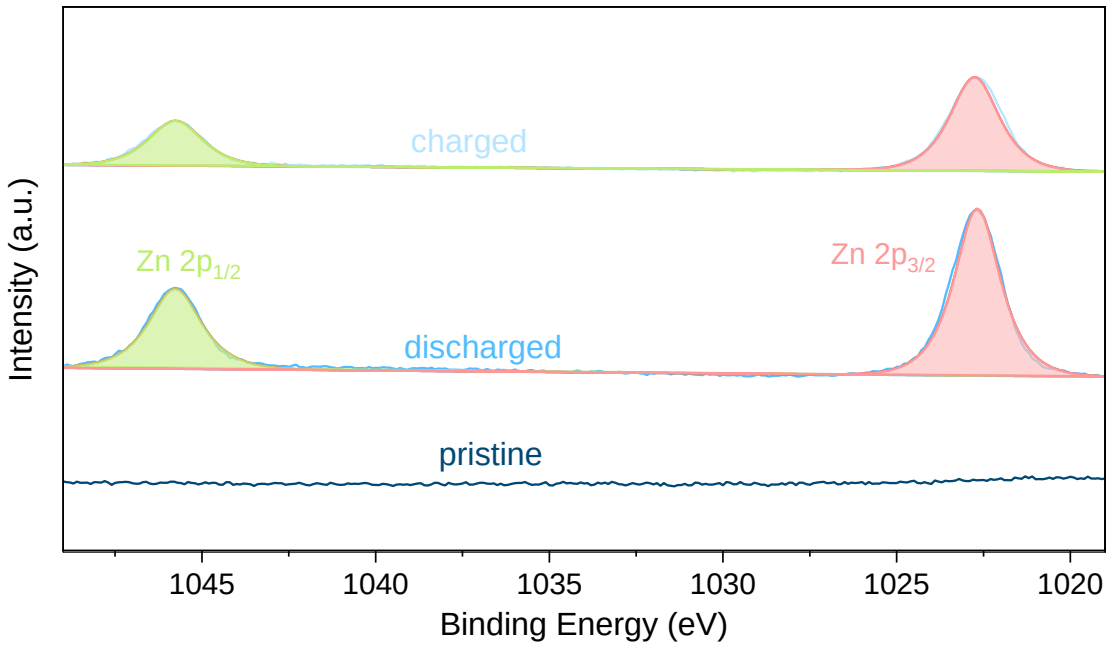

Figure S20. *Ex-situ* XPS spectra of Zn 2p of HAVO-11.0 electrode.

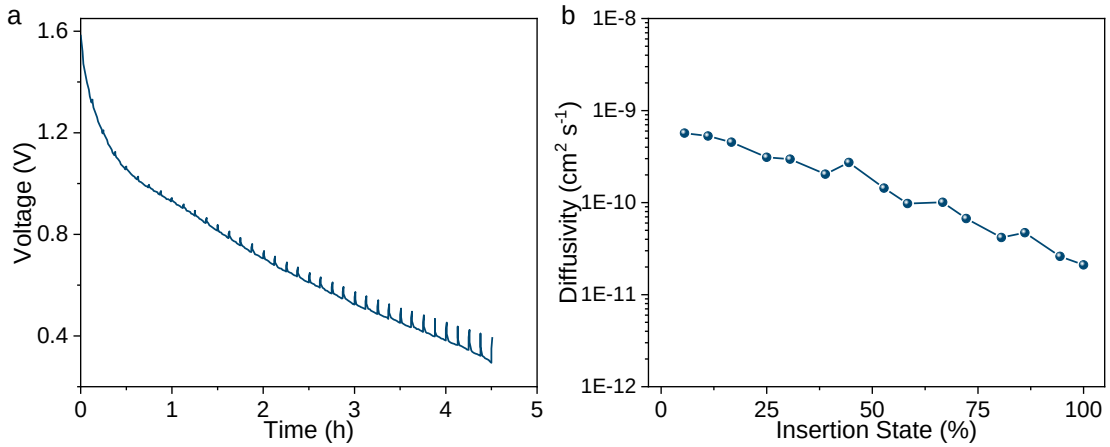

Figure S21. (a) GITT curves and (b) Diffusivity versus state of discharge of HAVO-11.0.

References

[1] J. P. Perdew, K. Burke, M. Ernzerhof, Generalized Gradient Approximation Made Simple, *Phys Rev Lett*, **1996**, *77*, 3865-68.

[2] D. Vanderbilt, Soft self-consistent pseudopotentials in a generalized eigenvalue formalism, *Phys Rev B Condens Matter*, **1990**, *41*, 7892-95.

[3] N. Govind, M. Petersen, G. Fitzgerald, D. King-Smith, J. Andzelm, A generalized synchronous transit method for transition state location, *Computational Materials Science*, **2003**, *28*, 250-58.

[4] T. A. Halgren, W. N. Lipscomb, The synchronous-transit method for determining reaction pathways and locating molecular transition states, *Chemical Physics Letters*, **1977**, *49*, 225-32.

[5] S. Smidstrup, A. Pedersen, K. Stokbro, H. Jonsson, Improved initial guess for minimum energy path calculations, *J Chem Phys*, **2014**, *140*, 214106.